AIAA 80-1012R

Helicopter Rotor Thickness Noise

Claude Dahan* and Edmond Gratieux*
Office National d' Etudes et de Recherches Aérospatiales, Châtillon, France

The attention is focused on rotor blade thickness noise (flow subsonic everywhere). The solution of the wave equation is written in a closed form (frequency domain) which emphasizes the essential parameters for this field. On another side, starting from an estimation of the loads on the rotor disk (lifting-line theory), the acoustic emission due to loads is estimated in such a way that we can compare the acoustic efficiency of blade thickness and loads. To compare experimental results and predictions, an original signal processing method was designed, which compensates the Doppler effect due to the helicopter motion.

Nomenclature

a = surface of blade section
A = modified angle, Eq. (16)
$\mathfrak{A}(z)$ = Airy function of argument z
B = number of blades
c = speed of sound
$F_{x,y,z}$ = loads on a blade
f = chordwise repartition of loads
G = Green's function
h = thickness of a blade
H = height of a microphone above the ground
$J_m(z)$ = Bessel function of order m
k = wave number
l = coordinate along the chord of a blade section
M = advancing Mach number
M_R = rotational tip Mach number
m = order of harmonics
p_e = acoustic pressure, due to thickness
$(p_e)_m$ = mth harmonic of p_e
p_L = acoustic pressure due to loads
$(p_L)_m$ = mth harmonic of p
p_d = direct pressure
p_r = reflected pressure
r = span coordinate
S = modified distance, Eq. (8)
$t,\tau,\hat{t}$ = time
V = velocity of the aircraft
V_l = velocity relative to the blade
V_n = velocity normal to the blade
x,y,z = coordinates of the observer
x_0,y_0,z_0 = coordinates of a source point
α = angle of the incident and reflected rays with the ground
β^2 = Lorentz factor: $1-M^2$
Φ,θ_b = angles (Fig. 1)
φ = phase angle, Eq. (16)
$\Delta\Phi$ = phase difference
Ω = rotational speed
ρ_0 = air density

I. Introduction

THE noise of helicopter rotors due to the displaced fluid volume during the blade motion has been intensively studied in the last few years.[1-3] Generally, this source of noise is considered to become important when the flow on the advancing blade side is transonic. Nevertheless, for many helicopters operating at high advancing speed, the flow remains subsonic everywhere, and the complexity of an acoustic prediction with the presence of a shock wave on the rotor disk is avoided. So, it would be interesting to get the noise field in a closed form, to stress easily the main parameters governing this field. A formula for predicting the part of noise due to blade thickness is thus derived.

The relative importance of this noise production mechanism is compared to other source mechanisms, especially to the fluid acceleration due to steady or unsteady loads on the rotor disk, loads computed with a lifting-line model.[4]

These predictions must be valided by experimental results; flyover noise records were analyzed, using an original signal processing method described later.

II. Thickness Noise Analytical Formulation

The solution of the convected wave equation, derived by Goldstein,[5] gives the pressure fluctuation in an integral form

$$p=\int_A \rho_0 V_n' \frac{DG}{D\tau}\,d\vec{y}+\int_A F_i\frac{\partial G}{\partial y_i}\,d\vec{y}+\int_v T_{ij}\frac{\partial^2 G}{\partial y_i \partial y_j}\,d\vec{y} \quad (1)$$

The field due to volume displacement effects is the first one

$$p_e=\int_A \rho_0 V_n' \frac{DG}{D\tau}\,d\vec{y} \quad (2)$$

This formula provides the noise for an observer moving with the aircraft, so that the medium is assumed to have a uniform velocity, equal (but of opposite sign) to the helicopter one. Then the integral of Eq. (2) must be evaluated when the source has the geometry of a rotor (Fig. 1).

A. Expression of the Field

If the speed modification V_n', normal to the blade, is a weak perturbation of the incident speed V_l (Fig. 1), then

$$V_n' = V_l\,(dh/dl) \quad (3)$$

Considering small values of the chordwise coordinate $l \ll S$ [see Eq. (8)], the Green's function can be replaced by the first terms of its Taylor series when $l \approx 0$, thus giving

$$p_e=\rho_0\int_{\text{rot.disk}} dS \int_{\substack{\text{blade}\\ \text{chord}}} V_n'\left(\frac{DG}{D\tau}\right)dl \quad (4)$$

$$=\rho_0\int_{\text{r.d.}} dS\int_{\text{b.c.}} |V_l|\,\frac{dh}{dL}\left[\left(\frac{DG}{D\tau}\right)_{l=0}+l\frac{\partial}{\partial l}\left(\frac{DG}{D\tau}\right)_{l=0}\right]dl \quad (5)$$

Presented as Paper 80-1012 at the AIAA 6th Aeroacoustics Conference, Hartford, Conn., June 4-6, 1980; submitted July 24, 1980; revision received March 11, 1981.

*Research Engineer.

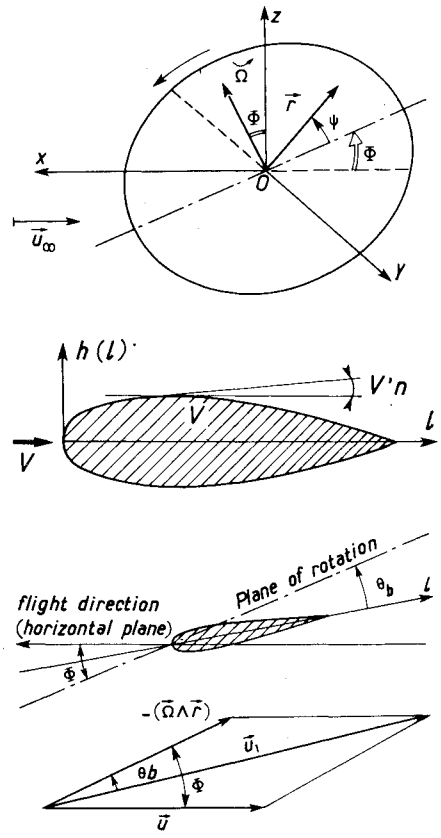

Fig. 1 Geometry of source region.

As

$$\int_{\text{b.c.}} \frac{\mathrm{d}h}{\mathrm{d}l}\,\mathrm{d}l = 0$$

and

$$\int_{\text{b.c.}} l\frac{\mathrm{d}\dot{h}}{\mathrm{d}l}\,\mathrm{d}l = a(r)$$

where $a(r)$ is the surface of a blade section, so

$$p_e = \rho_0 \int_{\text{r.d.}} \rho_0 |V_l| a(r) \frac{\partial}{\partial l}\left(\frac{\mathrm{D}G}{\mathrm{D}\tau}\right)_{l=0} \mathrm{d}S \tag{6}$$

B. The Green's Function

The Green's function derived by Garrick and Watkins,[6] for the propagation of an acoustic disturbance of pulsation ω in an uniform stream of velocity V_∞ can be used

$$G_\omega(x,y,z,t\,|\,x_0,y_0,z_0,\tau) = \frac{1}{4\pi S} e^{-ik\sigma} e^{i\omega(t-\tau)} \tag{7}$$

where

$$S = [(x-x_0)^2 + \beta^2[(y-y_0)^2 + (z-z_0)^2]]^{1/2}$$

$$\sigma = \frac{M(x-x_0)+S}{\beta^2} \tag{8}$$

$$\beta^2 = 1 - M^2$$

Then

$$\frac{\mathrm{D}G}{\mathrm{D}\tau} = \frac{\partial G}{\partial \tau} - V_\infty \frac{\partial G}{\partial x_0} = \frac{\partial G}{\partial \tau} + V_\infty \frac{\partial G}{\partial x} = -\frac{ikc}{\beta^2}\left(1 + \frac{Mx}{S}\right)G \tag{9}$$

So

$$\frac{\mathrm{D}G}{\mathrm{D}\tau} = -\frac{ikc}{\beta^2}\left(1 + \frac{Mx}{S}\right)G \tag{10}$$

C. Evaluation of the Operator $\partial/\partial l$

$\partial/\partial l$ can be resolved in parallel and perpendicular directions to the rotor disk (Fig. 1)

$$\frac{\partial}{\partial l} = \cos\theta_b \frac{1}{r}\frac{\partial}{\partial \Psi} + \sin\theta_b \frac{\partial}{\partial n} \tag{11}$$

To evaluate $\sin\theta_b$ and $\cos\theta_b$, the aerodynamic incidence is considered as equal to 0; as proved at the end of computation, the most radiative blade sections are at the tip, where the aerodynamic incidence is weak. Moreover, the axial and rotational induced velocities are considered small when compared to the tip blade relative velocity. The same types of assumptions were used by Arnoldi[7] for propellers. Then

$$\cos\theta_b = \frac{\Omega r + V_\infty \sin\Psi\cos\Phi}{|V_l|} \qquad \sin\theta_b = \frac{V_\infty \sin\Phi}{|V_l|} \tag{12}$$

$$\frac{\partial}{\partial n} = \cos\Phi\frac{\partial}{\partial z_0} + \sin\Phi\frac{\partial}{\partial x_0} = -\cos\Phi\frac{\partial}{\partial z} - \sin\Phi\frac{\partial}{\partial x} \tag{13}$$

we get

$$|V_l|\frac{\partial}{\partial l}\frac{\mathrm{D}G}{\mathrm{D}\tau}_{l=0} = -\frac{k^2c^2}{\beta^2}\left(1+\frac{Mx}{S}\right)\left[\left(1+\frac{V_\infty \sin\Psi\cos\Phi}{\Omega r}\right) + M\sin\Phi\left[\cos\Phi\frac{z}{S} + \left(M+\frac{x}{S}\right)\frac{\sin\Phi}{\beta^2}\right]\right]G \tag{14}$$

D. Far-Field Approximation

To compute the integral of Eq. (2), the far-field approximation must be introduced in Eq. (14). If

$$S_0 = [x^2 + \beta^2(y^2+z^2)]^{1/2}$$

$$\sigma_0 = \frac{Mx + S_0}{\beta^2}$$

it follows that

$$\sigma = \sigma_0 - \left(\frac{Mx_0}{\beta^2} + \frac{xx_0 + \beta^2(yy_0+zz_0)}{\beta^2 S_0}\right)$$

$$= \sigma_0 + r\left\{\cos\Psi\left[\left(M+\frac{x}{S_0}\right)\frac{\cos\Phi}{\beta_2} - \frac{z}{S_0}\sin\Phi\right] + \sin\Psi\frac{y}{S_0}\right\} \tag{15}$$

with

$$A\cos\varphi = y/S_0$$

$$A\sin\varphi = \left(M+\frac{x}{S_0}\right)\frac{\cos\Phi}{\beta^2} - \frac{z}{S_0}\sin\Phi \tag{16}$$

the Green's function (for its space dependence) becomes

$$G = \frac{1}{4\pi S_0} e^{-(ik/\beta^2)(Mx+S_0)} e^{-ikA\sin(\Psi+\varphi)} \tag{17}$$

E. Final Evaluation

Introducing Eq. (2) the result of Eqs. (6), (14), and (17), it remains to compute

$$p_e = -\frac{e^{-(ik/\beta^2)(Mx+S_0)}k^2c^2(1+Mx/S_0)}{4\pi\beta^2 S_0}\int_{R_0}^{R_1}\int_0^{2\pi} a(r) \times\left[1+\frac{V_\infty \sin\Psi\cos\Phi}{\Omega r}+M\sin\Phi\left(\cos\Phi\frac{z}{S_0}+M+\frac{x}{S_0}\right)\frac{\sin\Phi}{\beta^2}\right]e^{-ikAr\sin(\Psi+\varphi)}\,dr\,d\Psi \quad (18)$$

As usual, the interferences between blades are constructive only for the harmonics of the blade passing frequency, so that

$$k=mB\Omega/c \qquad (p_e)_m = B\cdot p_e \quad (19)$$

[$(p_e)_m$ stands for the mth Fourier coefficient in the complex Fourier series of the acoustic pressure.]

According to the properties of the Bessel functions $J_m(z)$, Eq. (18) is:

$$(p_e)_m = -\rho_0\frac{k^2c^2B}{4\pi\beta^2 S_0}\left(1+\frac{Mx}{S_0}\right)e^{-(ik/\beta^2)(Mx+S_0)+imB(\varphi+3\pi/2)} \times\left[\left(\int_{R_0}^{R_1} a(r)J_{mB}(kAr)\,dr\right)\left(1+M\sin\Phi\left(\cos\Phi\frac{z}{S_0}+\left(M+\frac{x}{S_0}\right)\frac{\sin\Phi}{\beta^2}\right)\right)+\tfrac{1}{2}V_\infty\frac{\cos\Phi}{\Omega}\int_{R_0}^{R_1}\frac{a(r)}{r} \times\left[e^{i(\pi+\varphi)}J_{mB+1}(kAr)-e^{-i(\pi+\varphi)}J_{mB-1}(kAr)\right]dr\right] \quad (20)$$

Here, we see a "homogeneous" part (term in $J_{mB}(kAr)$ and an "inhomogeneous" part ($J_{mB\pm1}$), essentially due to the nonuniformity of the incident speed seen by the blade during its rotation.

The inhomogeneous term vanishes if $V_\infty = 0$ (stationary flight) or if $\Phi=\pi/2$ (propeller case), where the general equation (20) becomes

$$(p_e)_m = -\frac{p_0k^2c^2B}{4\pi\beta^4 S_0}(i)^{mB}e^{-(ik/\beta^2)(Mx+S_0)}\left(1+\frac{Mx}{S_0}\right)^2 \times\int_{R_0}^{R_1} a(r)J_{mB}(kAr)\,dr \quad (21)$$

which is the expression given by Arnoldi[7] to predict the thickness noise of propellers.

III. The Acoustic Field

Equation (20) identifies the main parameters governing the thickness noise when the flow at the tip of the advancing blade approaches the transonic regime.

A. Directivity Patterns

Vertical Plane ($y=0$)

The field of Eq. (20) is governed by the functions J_{mB}, $J_{mB\pm1}$ with the argument $mB(\Omega r/c)A = mBM_R(r/R_1)A$, with the rotational tip Mach number $M_R=(\Omega R_1/c)$. When A can be replaced by its expression $[M+(x/S_0)](1/\beta^2)$. The space dependence of the field is then:

$$\approx\left(1+\frac{Mx}{S_0}\right)\left[J_{mB}\left(mBM_R\left(\frac{r}{R_1}\right)\left(M+\frac{x}{S_0}\right)\frac{1}{\beta^2}\right)\right]$$

$$\approx\left(1+\frac{Mx}{S_0}\right)\frac{\left[mBM_R\left(\frac{r}{R_1}\right)\left(M+\frac{x}{S_0}\right)\frac{1}{\beta^2}\right]^{mB}}{2^{mB}\,mB!} \quad (22)$$

and the acoustic pressure reaches its peak value at $x/S_0=1$ (when the observer is on the flight path, upstream of the rotor). Equation (22) also shows that the tip sections of the blades are the most radiative (i.e., $r=R_1$).

With $r=R_1$ and $x=S_0$, the argument of the Bessel functions becomes

$$mBM_R\frac{M+1}{1-M^2}=mB\frac{M_R}{1-M}$$

These functions increase rapidly when $M_R/(1-M)$ (the parameter used by Lowson[8]) approaches 1, i.e., when the flow on the advancing blade side is near the transonic regime

$$M_R/(1-M)\approx 1 \quad \Leftrightarrow \quad M_R+M\approx 1$$

Horizontal Plane ($z=0$)

A similar study of the field in the horizontal plane exhibits the same tendency (but less markedly): a concentration of the field in the flight direction. The main parameter is $M_R/(1-M)$[8], and the acoustic intensity diagram is more peaked as this ratio approaches 1.

B. Spectral Shape

These characteristics of the pressure field suggest an analogy between the acoustic and the electromagnetic radiation of an electric charge in relativistic motion on a circle.[9] In the same way, the asymptotic expansion gives the bunch of blade passing frequency multiples which dominates when $M_R/(1-M)\to 1$.

This bunch is given by the Bessel functions behavior $J_{mB}[mB\cdot M_R/(1-M)]$ (at the field point $x=S_0, y=z=0$).

When

$$\epsilon = M_R/(1-M), 1-\epsilon \ll 1$$

$$J_{mB}(mB\epsilon)\approx\frac{1}{\sqrt{\pi}}\left(\frac{2}{mB}\right)^{1/3}\mathfrak{A}\left[\left(\frac{mB}{2}\right)^{1/3}(1-\epsilon^2)\right]$$

$\mathfrak{A}(z)$ is the Airy function of argument z. So that

$$(p_e)_m\alpha(mB)^{5/3}\mathfrak{A}\left[\left(\frac{mB}{2}\right)^{2/3}(1-\epsilon^2)\right]$$

Two possibilities are to be considered:

1) $mB \ll 2(1-\epsilon^2)^{-3/2}$. Then

$$p_m\alpha(mB)^{5/3}\mathfrak{A}(0)=0.65(mB)^{5/3}$$

the intensities of the first harmonics increase as $(mB)^{5/3}$.

2) $mB \gg 2(1-\epsilon^2)^{-3/2}$. Then

$$p_m\alpha(mB)^{5/3}\frac{e^{-[(mB/2)^2][(1-\epsilon^2)^3/2]}}{(1-\epsilon^2)^{1/4}(mB/2)^{1/6}}$$

and $\to 0$ when $m\to\infty$.

So the bunch of dominant harmonics is given by

$$mB\approx 2[1-\epsilon^2]^{-3/2}=2\left[1-\left(\frac{M_R}{1-M}\right)^2\right]^{-3/2} \quad (23)$$

This shows that, for a four-bladed helicopter and for $M_R/(1-M)\lesssim 0.8$, the first harmonics remain dominant.

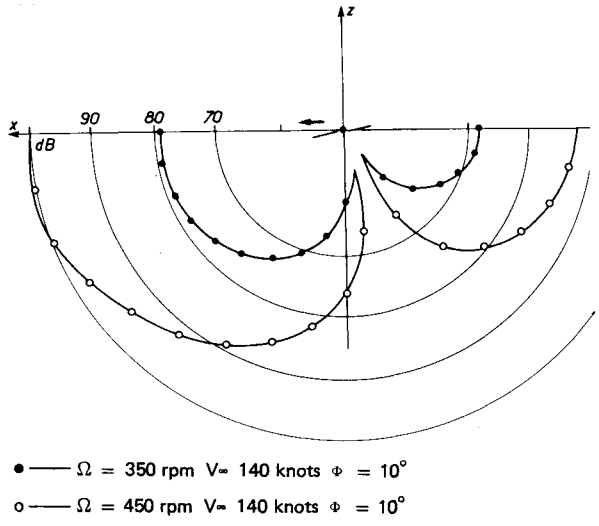

Fig. 2 Vertical directivity pattern for thickness noise field.

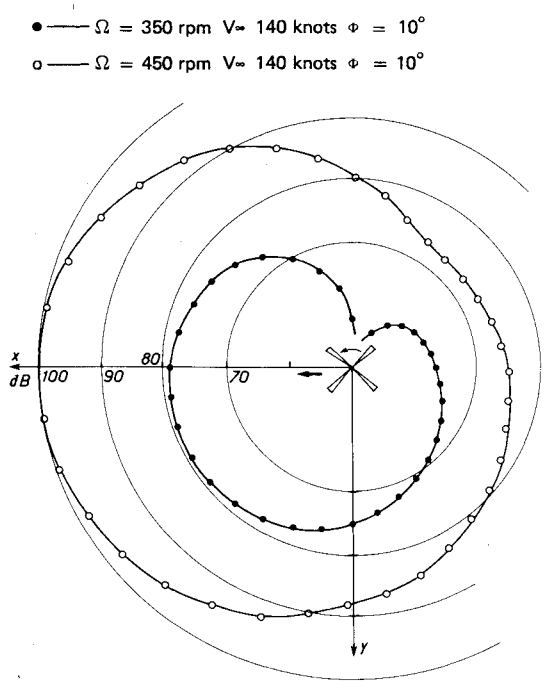

Fig. 3 Horizontal directivity pattern for thickness noise field.

IV. Numerical Results

Figures 2-5 were obtained by computing Eq. (20), with the following operating conditions: 1) $\Omega = 350$ rpm, $V_\infty = 140$ knots, $\Phi = 10$ deg, and rotor radius = 5.15 m. With vertical directivity (Fig. 2), the strongest lobe is in the flight direction, the peak intensity in the rotor plane. Horizontal directivity (Fig. 3) shows a dissymmetry only between the advancing and the retreating blade sides. The spectral shape is shown in Fig. 4. Note that at the peak intensity field point, the harmonic amplitudes decrease with the harmonic order (Sec. III B). The signal (Fig. 5) is shaped like a negative pulse but not very peaked (shape associated to the thickness noise phenomenon by Schmitz et al.[1]).

2) $\Omega = 450$ rpm, $V_\infty = 140$ knots, $\Phi = 10$ deg, and rotor radius = 5.15 m. The order of the highest harmonic is now $m \approx 3$. This spectral shape corresponds to a signal exhibiting a negative pulse narrower than in the previous case (Fig. 1). There, these last results must be used cautiously as the flow on the advancing blade tip is likely a local supersonic one.

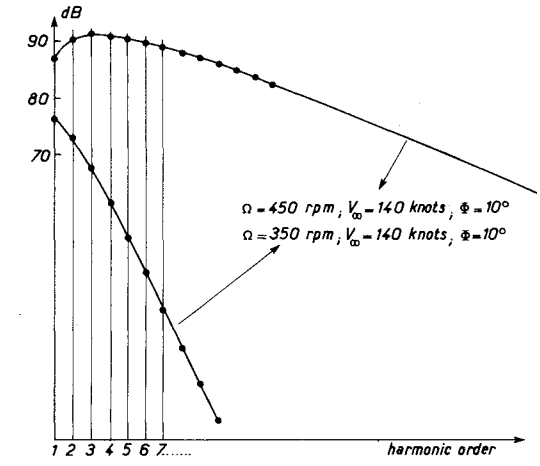

Fig. 4 Spectral shapes.

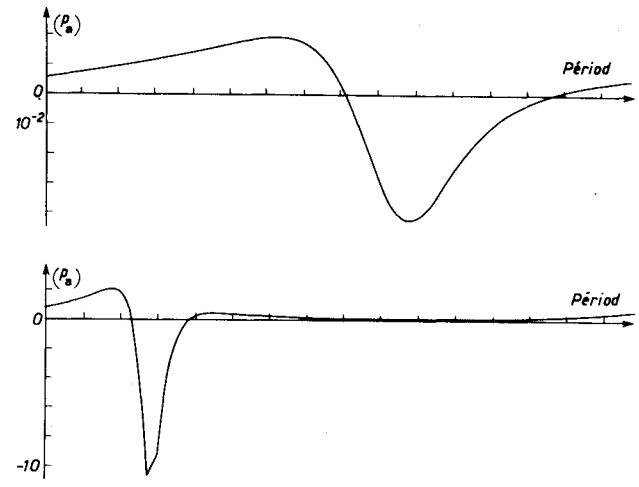

Fig. 5 Signal shape.

It remains now to compare the thickness noise field to the acoustic field due to loads, in order to assess the relative importance of these two components.

V. Loading Noise

A. Analytical Formulation

To evaluate the acoustic field due to loads, a well-known formula,[5] modified to account for the aircraft motion was used:

$$(p_L)_m = \frac{B}{2S_0} e^{-(ik/\beta^2)(Mx+S_0)} E_i \sum_{s=-\infty}^{+\infty} e^{i(mB+s)(\pi+\varphi)}$$

$$\times \int_{R_0}^{R_1} F_i^{(s)}(r) f_R^{(mB+s)}(r) J_{mB+s}(kAr)\,dr$$

Where E_i are the vector components defined by

$$E_x = -(ik/\beta^2)(M + x/S_0)$$

$$E_y = -iky/S_0$$

$$E_z = -ikz/S_0$$

$F^{(s)}_{x,y,z}(r)$ is the sth Fourier coefficient of the loads at the span r, and $f_R^{(s)}$ the sth Fourier coefficient of the chordwise repartition function of these loads (acoustic solidity func-

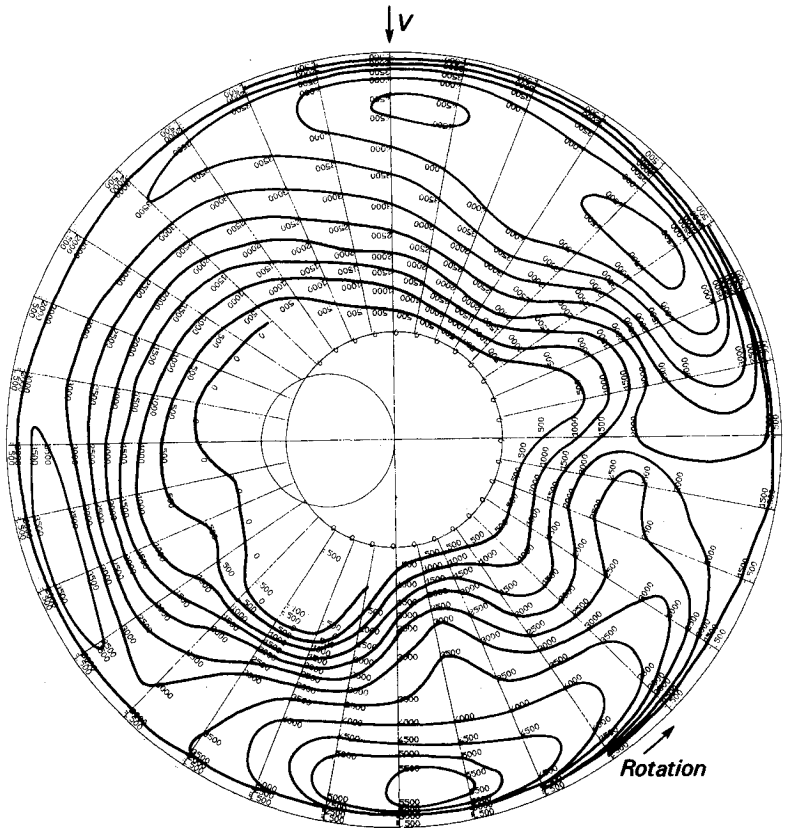

Fig. 6 Map of the force normal to the blade.

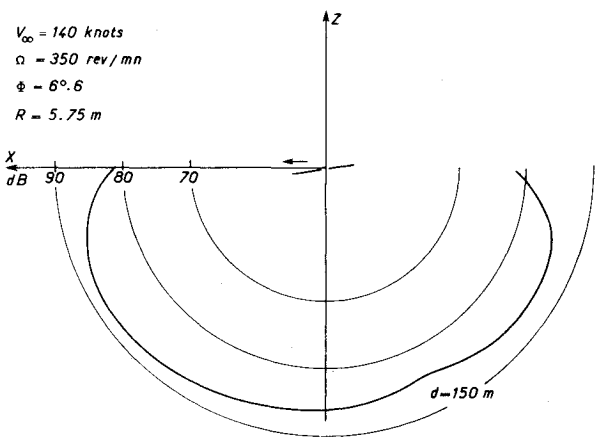

Fig. 7 Vertical directivity pattern for the loading noise.

tion).† Here, the steady and unsteady loads are necessary as an input for Eq. (24).

B. Blade Loads

With a particular operating set of parameters ($\Omega = 350$ rpm, $V_\infty = 140$ knots, $\Phi = 6.3$ deg, rotor radius $= 5.75$ m) characteristic of an actual helicopter flight, a lifting-line model computer code[4] gave the maps of the loads (Fig. 6). Applying well-known frame transformations[11] to the forces perpendicular and parallel to the blade elements, the loads $F_{x,y,z}$ were obtained.

†Let us note, incidentally, that a careful examination of the chordwise repartition effects has convinced us that f_R^{mB+s} must be used, instead of f_R^{mB},[10] which is a small correction considering the low solidity of a helicopter rotor.

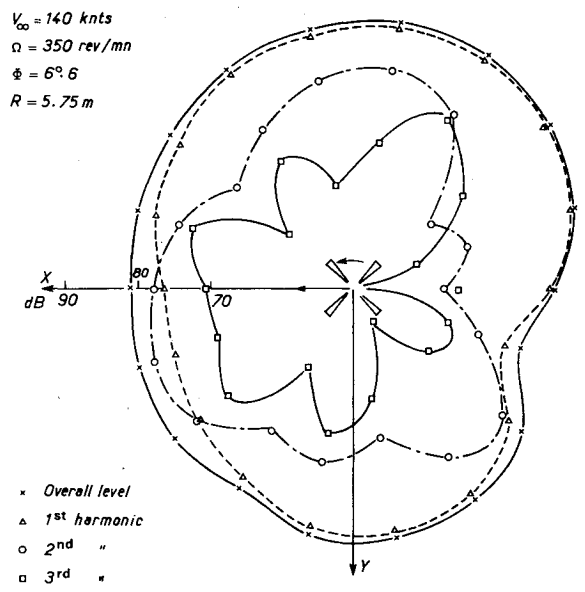

Fig. 8 Horizontal directivity pattern for the loading noise.

C. The Acoustic Field

These estimations of the loads F, and a rectangular shape for the chordwise repartition function f_R in Eq. (24) are introduced in a computer code, the output of which is the acoustic pressure at any field point. Some of the results are shown in Figs. 7 and 8.

Figure 7 shows the acoustic intensity directivity diagram in a vertical plane, the shape of which is similar to the common predicted one.[8] The intensity is slightly higher in the forward direction, by convection effects due to the aircraft motion. In the horizontal plane (Fig. 8), this acoustic intensity is at a

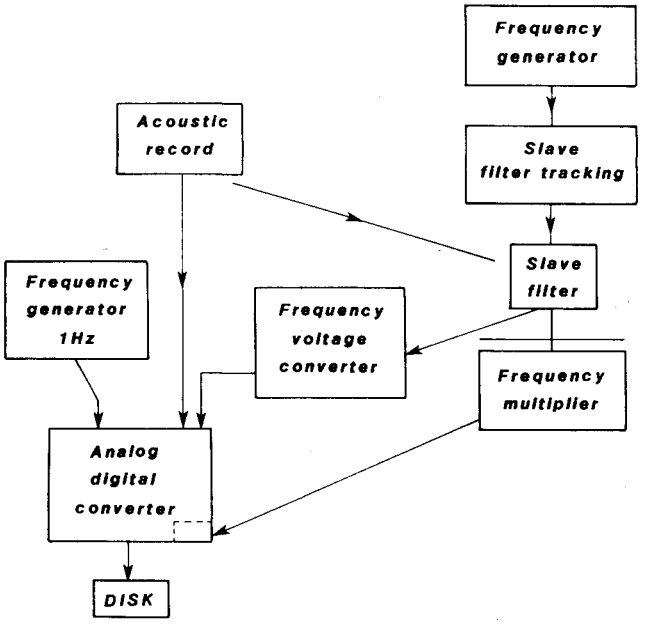

Fig. 9 Flyover noise analysis arrangement.

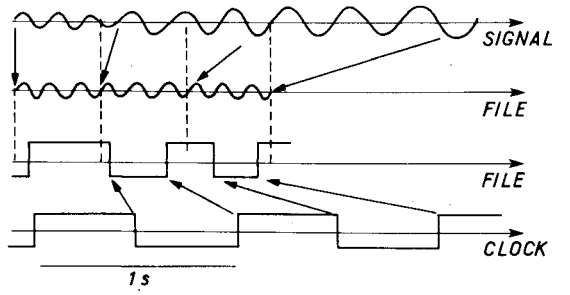

Fig. 10 Doppler effect compensation.

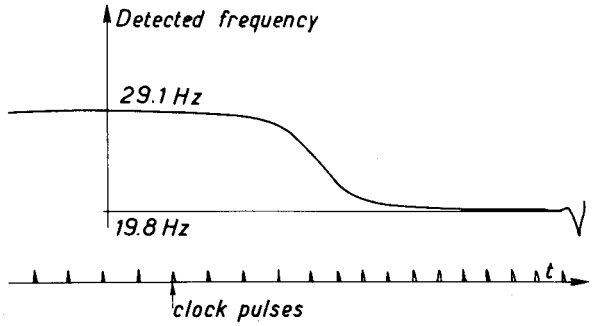

Fig. 11 Evolution of the detected frequency.

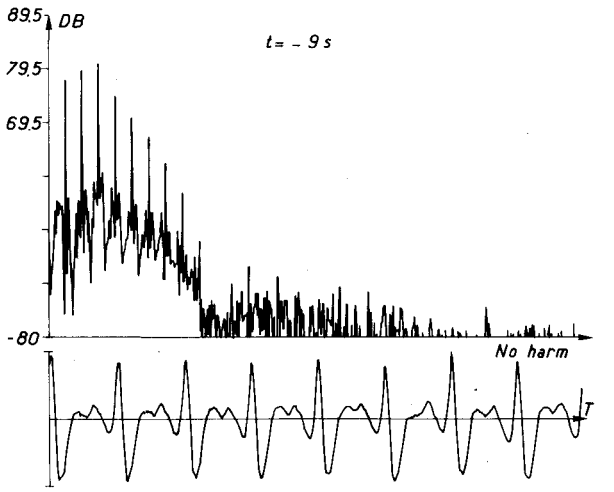

Fig. 12 Flyover noise spectrum and signal.

maximum on both sides of the flight path, as the peak in loads fluctuating amplitude appears when the blades are parallel to flight path (see Fig. 6).

The models retained to describe the acoustic field emitted by the rotor of a helicopter in horizontal, constant speed flight must now be experimentally validated. The analysis of a signal perceived by a ground-fixed microphone during a flyover directly provides the needed experimental data.

VI. Flyover Noise Analysis

The signal processing method to be used must compensate the advancing Doppler effect, thus avoiding the difficulty of coupling the acoustic signal with optical information coming from, for instance, theodolites. This compensation will be reached if all of the rotor noise tones appear at fixed positions when performing the signal Fourier analysis (a specified elementary filter in the spectral will correspond to a given tone). Moreover, detection of the time shift of any of these tones (due to the Doppler effect) is equivalent to following the aircraft motion.

An adapted sampling rate of the acoustic signal is to be built in three operations: 1) detection of a source characteristic frequency (time evoluting), 2) synchronization of the sampling rate on the detected frequency (frequency multiplication), and 3) Fourier analysis driven by the previous numerization.

A file containing three information sets can be made up of detected frequency evolution, acoustic signal sampled at a rate multiple of the detected frequency, and clock information. To get the two first sets, the operating procedure is summarized in Fig. 9:

1) The acoustic record is filtered through a low-pass filter to avoid spectra aliasing in the following Fourier analysis.

2) Then the signal goes to a slave filter to select the pure tone to be detected, which enters, on one side, a frequency-voltage converter, the output of which is a dc signal proportional to the frequency; and, on the other side, a frequency multiplier giving a square wave signal, the repetition rate of which defines the sampling of the noise signal. The acoustic record and the dc voltage are then sampled, and stored on a disk.

Each constitutive file block contains a fixed number N of signal values [the block size N is related to the number of elementary filters in the Fourier analysis $(N/2)$]. The time elapsed between two following blocks depends on the sampling rate and on the block size retained (Fig. 10). A table is thus necessary to convert this artificial time ("file" time) into the observer's time. For this, a clock signal (squares at a rate of 1 Hz) is sampled simultaneously with the acoustic signal and the frequency evolution dc voltage (defined previously), at the same sampling rate (variable) (Fig. 10).

Here are some results, where this procedure is applied to a flyover acoustic signal recorded by SNIAS, the microphone being at a certification position (height above the ground $H = 1.2$ m). The detected frequency varies from $f_1 = 29.1$ Hz to $f_2 = 19.8$ Hz (Fig. 11).

In the source frame, $f_0 = (2f_1f_2)/(f_1+f_2) = 22.6$ Hz, by far close to the frequency deduced from the operating conditions ($f_0 = 23.3$ Hz). The risk of error due to the frequency detection thus appears weak. Then the Fourier transformation of each block of the file was performed.

In Fig. 12, the perception time of the spectrum presented (it is easy, knowing the reception time, to compute the emission time and thus to determine the aircraft's position when the analyzed signal sample was emitted); the signal time history associated to the spectrum is also drawn. Recasting all the power spectral densities, the time evolution of a prescribed

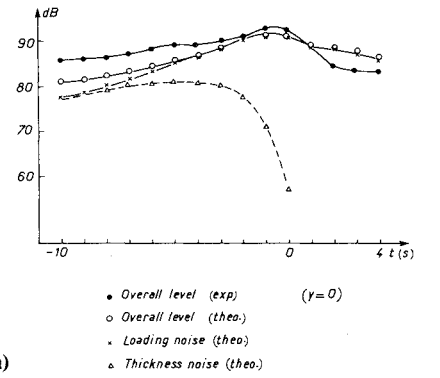

a)

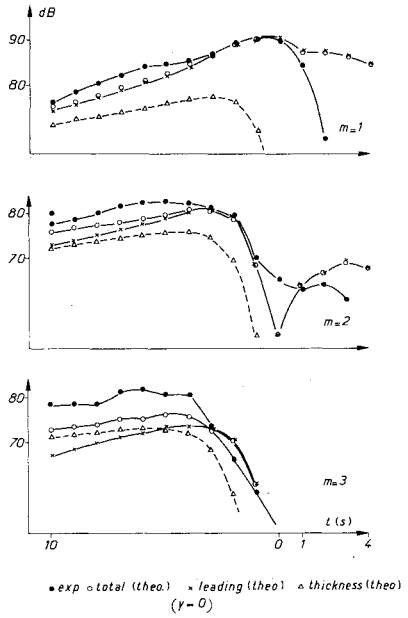

b)

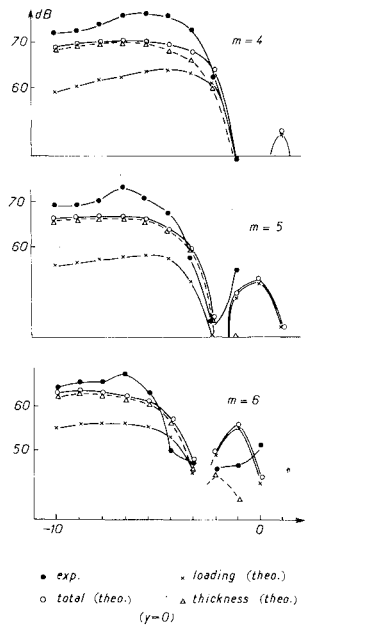

c)

Fig. 13 a) Predictions/experiments comparisons; b) and c) harmonic levels.

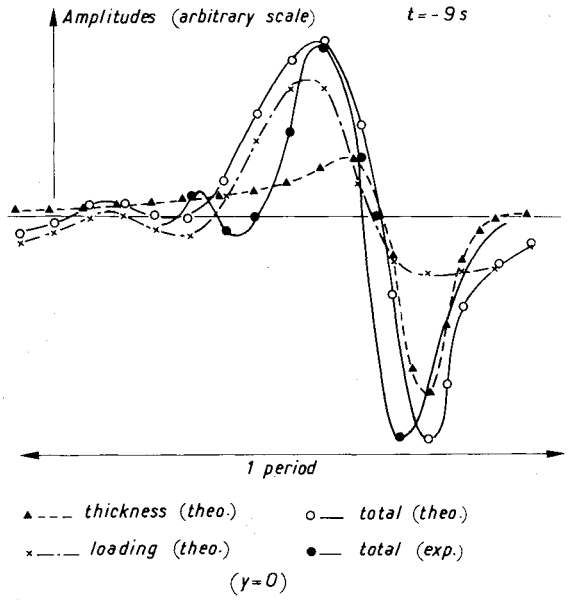

Fig. 14 Comparison of pulses shape (theory/experiment).

rotor harmonic is known (Fig. 13) quite easily; the signal cancellations due to ground reflections are clearly distinguishable. Then, these results are to be compared to the outputs of the prediction schemes derived in Secs. II and III.

VII. Experiment/Theory Comparisons

Equations (20) and (24) include the amplitude effects due to the aircraft motion, so that to get the field for a moving observer relative to the aircraft (ground fixed), it is necessary only to introduce in Eqs. (20) and (24) the instantaneous position of this observer in the helicopter frame:

$$p(t)=p[x(t),y(t),z(t),t]$$

The instantaneous frequency perceived is the phase derivative of $p(t)$ with respect to time t. When the observer is at a height H above the ground, some changes in the predictions schemes are needed, considering ground reflection phenomena. So, we assume, for the studied low frequencies, that the ground acts as a perfectly reflecting surface and that at the observer's position, the waves are locally plane. Then, for each field p_e, p_l, the pressure resulting from direct (p_d) and reflected (p_r) rays is computed.

$$p=p_d(t)+p_r(t)=p_d(t)\,[1+Re^{i\Delta\Phi}]$$

The phase $\Delta\Phi$, linked to the emission position of the aircraft via the incidence angle α, must be evaluated at the retarded time $\hat{t}$, and depends also on the perceived frequency f

$$\Delta\Phi(\hat{t})=4\pi fH\sin\alpha(\hat{t})/c$$

Then modifying the computer codes, theoretical estimations are directly comparable to experimental results.

The analyzed operating conditions are given in Sec. III; three microphones were chosen to provide the experimental data. First, is considered the microphone placed under the flight path. Experiments and predictions fit correctly before the overhead point ($t=0$), but not after. This discrepancy is likely due to the loading noise computation scheme. The harmonics evolution during the flyover before the overhead position shows that the first harmonic is essentially due to the loading noise phenomenon; for the second, loads and thickness are equally important; for higher harmonics, the thickness mechanism is dominant. The major misfit theory/experiments arises for the third harmonic of the blade passing frequency (Fig. 14).

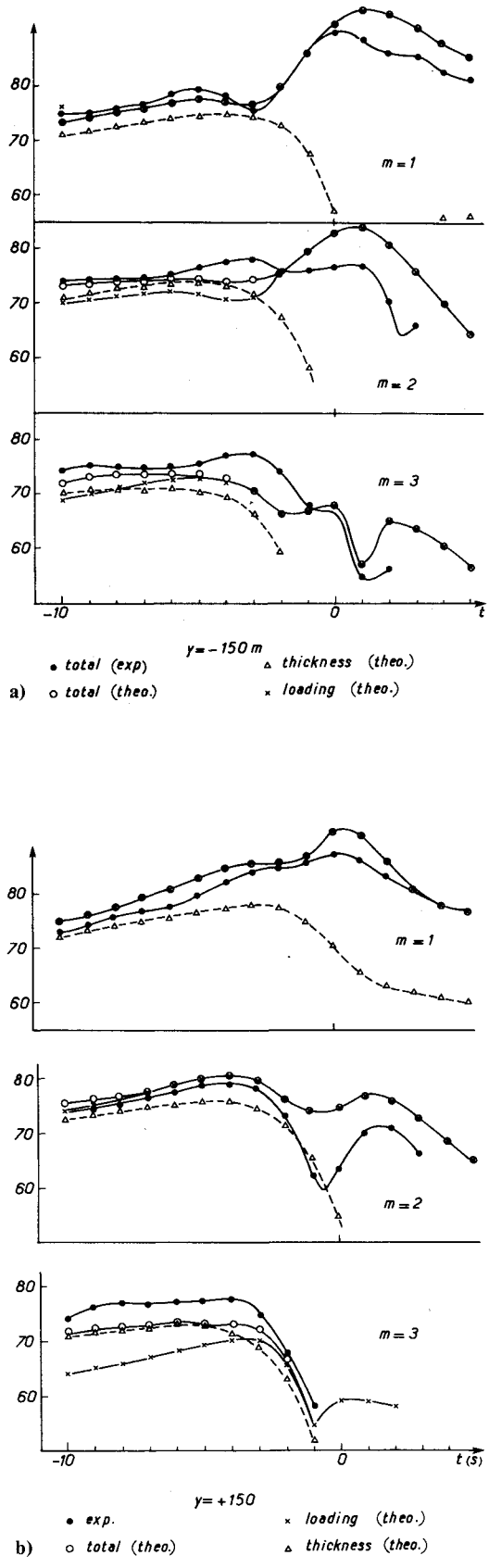

Fig. 15 Harmonic levels.

Comparing theoretical and experimental shapes of the periodic pulses generated by the rotor (Fig. 14), a correct agreement exists, except for the positive peak (due to loads) larger than the measured one, and for the negative computed peak (due to thickness) slightly shifted in time. The conclusions are the same considering the other microphones, in lateral positions with respect to the flight path (Fig. 15).

VIII. Conclusion

A theoretical model was used to derive an explicit formulation for the "thickness" acoustic field generated by a helicopter rotor operating at high subsonic conditions. This formulation enables us to point out the essential features of this field.

Starting from a map of the loads on the blades, a computer code gave the noise field associated to the loading phenomenon. Nevertheless, these last estimations need to be taken cautiously because the lifting-line model retained to build up the loads map is limited to the sixth harmonic of the rotational frequency. To compare the results of these prediction schemes to experimental data, the noise field perceived by a ground observer during a flyover was analyzed, the ground reflection phenomenon being taken into account through a rather crude model (perfectly reflective surface).

Before the overhead position, the thickness mechanism seems to be dominant for the highest blade passing frequency harmonics in the acoustic signal ($m \geq 3$), the first harmonic being generated in the whole space by the loading mechanism.

These results must be completed by:

1) A better account for the higher harmonics of loads fluctuations (discrepancy after the overhead position) and for the ground reflection properties.

2) An examination of the new mechanism arising when the flow on a blade becomes transonic, a complicated situation completely ignored in this paper.

References

[1] Schmitz, F. H. and Yu, Y.H., "Theoretical Modelling of High Speed Impulsive Noise," *Proceedings of 3rd European Rotorcraft and Lift Powered Aircraft Forum,* Aix-en-Provence, 1977.

[2] Schmitz, F.H. and Boxwell, D.A., "In Flight Far Field Measurements of Helicopter Impulsive Noise," *Proceedings of 32nd Annual National V/STOL Forum of the American Helicopter Society,* 1976.

[3] Hawkings, D.L., "Noise Generation by Transonic Open Rotors," *Proceedings of the I.U.T.A.M. Symposium,* Göttingen, Fed. Rep. of Germany, 1979.

[4] Costes, J.J., "Rotor Response Prediction with Nonlinear Aerodynamic Loads on the Retreating Blade," *Vertica,* Vol. 2, 1978, pp. 73-85.

[5] Goldstein, M.V., "Aeroacoustics," NASA-SP 346, 1974.

[6] Garrick, I.E. and Watkins, C.E., "A Theoretical Study of the Effect of Forward Speed on the Sound Pressure Field around Propellers," NACA TM 3018, 1953.

[7] Arnoldi, A., "Thickness Noise of Propellers," NACA TN 0.8096-1, 0.8096-2, 1958.

[8] Lowson, M.V. and Ollerhead, J.B., "A Theoretical Study of Helicopter Rotor Noise," *Journal of Sound and Vibration,* Vol. 9, No. 2, 1969.

[9] Landau, L. and Lifchitz, E., *Théorie du Champ,"* ed. Mir, Moscow, 1966.

[10] Revell, J.D. and Griffith, E.D., "Low Noise Propeller Technology," AFAPL, TR-73-115, Dec. 1973.

[11] Loewy, R.G. and Sutton, L.R., "A Theory for Predicting the Rotational Noise of Lifting Rotors in Forward Flight, including a Comparison with Experiments," *Journal of Sound and Vibration,* Vol. 4, No. 3, 1966.